 CMES, vol.19, no.3, pp.181-196, 2007

Mesoscopic Simulation of Binary Immiscible Fluids Flow in a Square Microchannel with Hydrophobic Surfaces

S. Chen[1,2], Y. Liu[1,3], B.C. Khoo[4], X.J. Fan[5] and J.T. Fan[6]

Abstract: The mesoscopic simulation for fluids flow in a square microchannel is investigated using dissipative particle dynamics. The velocity distribution for single fluid in a square channel is compared with the solutions of CFD solver, which is found to be in good agreement with each other. The no-slip boundary condition could be well held for the repulsive coefficient ranged from 9.68 to 18.0. For the same range of repulsive coefficient, various wettabilities could be obtained by changing the repulsive coefficient for binary immiscible fluids, in which the immiscible fluids are achieved by increasing the repulsive force between species. The typical motion of the DPD particle might be described as Brownian, which is similar to MD simulation results. The DPD simulated fluid/fluid interfacial tension is in accord with theoretical prediction. For the same repulsive parameters, the fluid/solid interfacial tension is always greater than the fluid/fluid interfacial tension. The DPD simulated static contact angles are in good agreement with Young's equation even though some differences exist due to thermal fluctuation. For moving contact line, the advancing and receding contact angles are different with each other. It is found that the cross-section area of hydrophobic fluid retracts towards the central part of the square microchannel and forms a circle. The retraction extent of the hydrophobic fluid is dependant on the velocity itself. For immiscible fluid, the moving velocities of fluid A in a microchannel could be increased by increasing the repulsive coefficient between fluid A and walls, and larger static angle may produce larger moving velocity.

Keyword: Dissipative particle dynamics; Microchannel; Immiscible binary fluids

1 Introduction

In the past decade, microfluidics have been found increasing applications in a variety of industrial fields. For example, emulsification is an important structure-forming process applied in the food, pharmaceutical, and cosmetics industry, and microchannel emulsification has been a novel technique for producing monodispersed emulsions in which droplets formed by spontaneous transformation caused by interfacial tension (Abrahamse et al. 2001; Sugiura et al. 2002a & 2002b; Vladisavljevic and Williams 2005). Furthermore, the ability to control surface tension promises a new powerful actuation mechanism for microelectromechanical systems (MEMS) because of the advantageous scaling effect of the surface tension in microscale (Lee and Kim 2000). On the other hand, hydrophilic-hydrophobic patterning is used by a variety of biosystems to direct the motion of fluids at surfaces, such as steering the motion of fluid droplets in liquid microchips (Gau et al. 1999 and Kuksenok et al. 2002). However, the rapid progress in utilizing MEMS has not been matched by completely understanding of microscale flow behaviour and it is still an open problem (Croce and D'Agaro 2005; Tang et al. 2005).

[1] Department of Mechanical Engineering, The Hong Kong Polytechnic University, Hung Hom, Kowloon, Hong Kong
[2] School of Mechanical and Power Engineering, Shanghai Jiaotong University, Shanghai, P. R. China, 200030
[3] Corresponding author. E-mail: mmyliu@polyu.edu.hk
[4] High Performance Computation for Engineered System, Singapore-MIT Alliance, National University of Singapore, Singapore 117576
[5] Cooperative Research Centre for Polymers, 32 Business Park Drive Notting Hill, VIC 3168, Australia
[6] Institute of Textile and Clothing, The Hong Kong Polytechnic University, Hung Hom, Kowloon, Hong Kong

In order to understand the physics involved in the operation and manufacture of small devices, it is important to develop predictive models that reveal the thermodynamic behavior and hydraulic performances of complex fluids in micron-sized channels. One of the challenges inherent in modelling such a complex system is incorporating not only the interactions between the components but also, the interactions between the fluid and the substrate, i.e., wettability and surface tension, which play a dominate role in the behavior of confined fluids (Kuksenok et al. 2003).

Though Brownian dynamics simulation (BDS) (Hur et al. 2000), Lattice Gas Automata (LGA) (Frisch et al. 1986) and Lattice Boltzmann (LB) (Suppa et al. 2002) are mesoscale simulation methods, it is difficult for BDS to deal with complex flow field and for LGA and LB to cope with complex fluids. Dissipative particle dynamics (DPD), which was introduced by Hoogergrugge and Koelman (1992), is a potentially very effective approach in simulating mesoscale hydrodynamics with its basis in statistical mechanics founded by Español and Warren (1995), and Marsh (1998). DPD facilitates the simulations of static and dynamics complex fluid systems on physical interesting length and time scales. The DPD model consists of particles that correspond to coarse-grained entities, thus, representing molecular clusters rather than individual atoms (Pivkin and Karniadakis, 2005). The particles move off-lattice interacting with each other through a set of prescribed and velocity-dependent forces.

DPD has been successfully used to model rheologically complex liquids (Zhang et al. 1997; Chen et al. 2004), including interfaces. For binary immiscible fluid systems, Novik et al. (1997) investigated the domain growth and phase separation using DPD. Clark et al. (2000) performed simulations of a pendant drop and a drop in simple shear flow. Chen et al. (2004) investigated the steady-state and transient shear flow dynamics of polymer drops in a microchannel using the DPD method. Liu et al. (2004) simulated a process measuring the interfacial tension of polymers by means of DPD. Jones et al. (1999) studied the dynamics of a semi-infinite surface-confined drop in a simple shear field. A drop exists as a spherical cap on a planar solid surface when in the absence of gravity.

However, as for what we know, at present there is no further research work in DPD considering the flow behaviors of binary immiscible fluids in microfluidic channels, especially for plugs. The plugs, surrounded by immiscible carrier fluid, are defined as droplets that are large enough to touch the walls of the channel and do not wet the walls (Bringer et al. 2004). The surface is said to be hydrophobic if static contact angle is larger than 90^o. In the present study, the DPD method is used to investigate the binary immiscible fluids (plugs) flow in a three-dimensional (3D) square microchannel with hydrophobic surfaces. Firstly, the velocity distributions in a square microchannel for the simple DPD fluid are compared with those of CFD solver. The imposed no-slip boundary condition is verified for various fluid/solid repulsive parameters. Then, the interfacial tensions for fluid/fluid and fluid/solid are computed using the Irving-Kirkwood equation. The immiscible fluids are achieved by increasing the repulsive force between species. The static and dynamic contact angles are simulated and their relationship with repulsive parameters is discussed. The moving velocities for plugs in square microchannel are analysed for surfaces with various static contact angles.

2 Numerical Methods

2.1 Dissipative particle dynamics (DPD)

In DPD method, three inter-particle forces, dissipative, random and conservative forces, act upon the particles. Dissipative and random forces combine to create a continuous "fluid" in which the particles are suspended and free to interact hydrodynamically. Conservative forces reduce the possibility of overlapping for particles (Elliott and Windle, 2000). Each particle moves along its new velocity for a time-step after a possible collision of two particles. In detail, the DPD system consists of a set of interaction particles, governed by Newton's equations of motion - for a simple DPD

particle i,

$$\frac{d\mathbf{r}_i}{dt} = \mathbf{v}_i, \quad \frac{d\mathbf{v}_i}{dt} = \mathbf{f}_i + \mathrm{F}_e, \tag{1}$$

where $\mathbf{r}_i$ and $\mathbf{v}_i$ are the position and velocity vectors of particle i, $\mathbf{f}_i$ is the interparticle force on particle i by all of the other particles (except itself), and F_e is the external force. The dynamic interactions between the particles are composed of two parts: dissipative and stochastic. These complement each other to ensure a constant value for the mean kinetic energy of the system. The unit of mass is taken to be the mass of a particle, so that the force acting on a particle equals its acceleration. The force $\mathbf{f}_i$ contains three parts, each of which is pairwise additive:

$$\mathbf{f}_i = \sum_{j \neq i} (\mathbf{F}_{ij}^{\mathrm{C}} + \mathbf{F}_{ij}^{\mathrm{D}} + \mathbf{F}_{ij}^{\mathrm{R}}), \tag{2}$$

where the sum runs over all other particles within a certain cut-off radius $\mathbf{r}_{\mathrm{C}}$. In the present study $\mathbf{r}_{\mathrm{C}}$ is taken as the unit of length.

Since the time average of the dissipative and fluctuation forces is zero, they do not feature in the equilibrium behaviour of the system, which is governed solely by conservative forces. The conservative force $\mathbf{F}_{ij}^{\mathrm{C}}$ is a soft repulsion acting along the line of centres and is given by

$$\mathbf{F}_{ij}^{\mathrm{C}} = \begin{cases} a_{ij}(1 - r_{ij}/r_{\mathrm{C}})\hat{\mathbf{r}}_{ij} & (r_{ij} < r_{\mathrm{C}}), \\ 0 & (r_{ij} \geq r_{\mathrm{C}}). \end{cases} \tag{3}$$

where a_{ij} is a maximum repulsion between particles i and j, and $\mathbf{r}_{ij} = \mathbf{r}_i - \mathbf{r}_j$, $r_{ij} = |\mathbf{r}_{ij}|$, $\hat{\mathbf{r}}_{ij} = \mathbf{r}_{ij} \Big/ |\mathbf{r}_{ij}|$.

The dissipative or drag force, $\mathbf{F}_{ij}^{\mathrm{D}}$, on particle i by particle j, is given by

$$\mathbf{F}_{ij}^{\mathrm{D}} = -\gamma w^{\mathrm{D}}(r_{ij})(\hat{\mathbf{r}}_{ij} \cdot \mathbf{v}_{ij})\hat{\mathbf{r}}_{ij}, \tag{4}$$

where w^{D} is an r-dependent weight function vanishing for $r > r_c$, $\mathbf{v}_{ij} = \mathbf{v}_i - \mathbf{v}_j$, γ is a coefficient which controls the extent of dissipation in a simulation time step. The negative sign in front of γ indicates that the dissipative force is opposite to the relative velocity $\mathbf{v}_{ij}$.

The dissipative force, acting against the particle motion, would reduce the kinetic energy of the system. This is compensated by the random motion produced by the stochastic force $\mathbf{F}_{ij}^{\mathrm{R}}$, given by

$$\mathbf{F}_{ij}^{\mathrm{R}} = \sigma w^{\mathrm{R}}(r_{ij})\xi_{ij}\hat{\mathbf{r}}_{ij}, \tag{5}$$

where w^{R} is also an r-dependent weight function vanishing for $r > r_c$, and ξ_{ij} is a Gaussian variable with zero mean and variance equal to Δt^{-1}, where Δt is the time step, and σ is a coefficient characterizing the strength of the random forces. These forces also act along the line of centres.

Español and Warren (1995) showed that either of the two weight functions appearing in Eq. (4) and Eq. (5) can be chosen arbitrarily; the other weight function is determined by

$$w^{\mathrm{D}}(r) = [w^{\mathrm{R}}(r)]^2, \tag{6}$$

$$\sigma^2 = 2\gamma k_{\mathrm{B}} T, \tag{7}$$

where $k_{\mathrm{B}}T$ is the Boltzmann temperature of the system. This is analogous to the fluctuation-dissipation theorem for the system (Huilgol and Phan-Thien, 1997) and ensures that the kinetic energy of the system is stabilized . Taking $k_{\mathrm{B}}T$ as the unit of energy, we have

$$\sigma^2 = 2\gamma. \tag{8}$$

We use the following weight function to improve on the Schmidt number for the system (Fan et al., 2006), instead of quadratic function, $(1 - r/r_c)^2$ which is usually adopted,

$$w^{\mathrm{D}}(r) = [w^{\mathrm{R}}(r)]^2 = \begin{cases} \sqrt{1 - r/r_{\mathrm{C}}} & (r < r_{\mathrm{C}}), \\ 0 & (r \geq r_{\mathrm{C}}). \end{cases} \tag{9}$$

This weight function yields a stronger dissipative force between particles than the standard quadratic force, for a given configuration of particles and interaction strength.

The updated velocities and positions of the particle can be calculated once the forces on the particle have been calculated. A modified velocity-Verlet (Groot and Warren, 1997) scheme was adopted in the present study, in which the force is still updated once per iteration with virtually no increase in computational cost. The computation

is carried out for each particle for a large number of time steps, sufficient to get convergence for the system properties, such as viscosity, pressure, and interfacial tension; they are obtained by taking relevant statistical averages of the positions, velocities or forces for each particle at each time step.

2.2 Binary immiscible fluids

Immiscible fluid mixtures exist because individual molecules attract similar and repel dissimilar molecules (Novik and Coveney, 1997). The miscibility of the two fluids is controlled mainly by the repulsive parameter a between fluids A and B. The immiscible fluids are achieved by increasing the repulsive force between species. In the present study, a new variable is introduced, called the "colour" according to Rothman-Keller (Novik and Coveney, 1997). Here, for example, red represents fluid A and blue represents fluid B. When two particles of different colours interact, we increase the conservative force, thereby increasing the repulsion, that is,

$$a_{ij} = \begin{cases} a_0 & \text{if particles } i \text{ and } j \text{ are the same color,} \\ a_1 & \text{if particles } i \text{ and } j \text{ are different colors.} \end{cases} \tag{10}$$

The two phases would be completely miscible if $a_1 \approx a_0$ and almost entirely immiscible if a_1 exceeds a_0 significantly.

Groot and Warren (1997) have made a link between the repulsive parameter a and χ-parameters in Flory-Huggins-type models. They pointed out that DPD model can simulate liquid-liquid and liquid-solid interfaces, and in this way the method is similar to the Flory-Huggins theory, and can in fact be viewed as a continuous version of this lattice model.

The parameter χ is positive when A and B are two immiscible components; when they are miscible over AA or BB contacts, then it is negative. If χ is very small and positive, no segregation will take place, but when it exceeds a critical value, A-rich and B-rich domains will occur. The critical point of χ-parameters could be calculated by Eq. (19) of Groot and Warren (1997). In the present study the parameters will be chosen where segregation takes place, i.e., $\chi > \chi^{\text{crit}}$. The Flory-Huggins parameter for monomers is obtained by Groot and Warren (1997). The calculated χ-parameter for two densities ($\rho = 3$ and 5) is expressed as a function of the excess repulsion parameter Δa, where $\Delta a = a_1 - a_0$. It is shown that for $\chi > 3$ there is a very good linear relation between χ and Δa. Explicitly, it is

$$\begin{aligned} \chi &= (0.286 \pm 0.002)\Delta a \ \ (\rho = 3), \\ \chi &= (0.689 \pm 0.002)\Delta a \ \ (\rho = 5). \end{aligned} \tag{11}$$

We fix the density at 4 for our DPD system, and use Eq. (11) as an effective mean for extrapolation to estimate the Flory-Huggins parameterχ.

2.3 Implementation of the boundary condition

It is well known that, at a macroscopic level, the boundary condition for a viscous fluid at a solid wall is so-called "no slip". The liquid velocity field vanishes at a fixed solid boundary. For most applications the no-slip condition may be accepted uncritically as a phenomenological rule. However, this condition is an assumption that cannot be derived from first principles and could, in theory, be violated. As shown in Lauge et al. (2005), the small-scale interactions between a liquid and a solid leads to extremely rich possibilities for slip behavior, with dependence on factors such as wetting conditions, etc. Using Molecular Dynamics (MD), Koplik et al. (1989) pointed out the no-slip boundary condition appears to be a natural property of a dense liquid interacting with a solid wall with molecular structure and interactions. But we know a serious problem arises when a contact line separating two immiscible fluids moves along a solid surface. The straightforward hydrodynamic analysis of this situation predicts a divergent energy dissipation rate. In fact, Barrat et al. (1999) used MD to consider the special case of a liquid that partially wets the solid (i.e., a drop of liquid, in equilibrium with its vapor on the solid substrate, has a finite contact angle). They showed that when the contact angle is large enough, the boundary condition can drastically differ (at a microscopic level) from a no-slip condition.

The no-slip condition is a statement about the continuum velocity and the time and space average of fluid molecules occupying a sampling region at the wall. When the fluid reacts with the wall, the (continuum, Eulerian) no-slip assumption provides no molecular information. A kind of mechanism, kinematically, is a rolling or caterpillar like motion of the molecules. This is analogous to a ball rolling on a plane, where the part of the ball touching the plane is instantaneously at rest but has nonzero acceleration and rolls off (Koplik et al., 1989). Because of the soft potentials employed in DPD, the simple no-slip boundary conditions are difficult to impose. Unlike the MD method, the soft repulsion between DPD particles cannot prevent fluid particles from penetration solid boundaries, and thus extra effort is required to impose accurately the no-slip wall boundary condition (Visser et al. 2005; Pivkin et al. 2005; Revenga et al. 1999; Duong-Hong et al. 2004; Willemsen et al. 2000; and Revenga et al. 1998). In the present study, we implement the boundary condition according to Fan et al. (2003). The solid wall is represented by using frozen particles. As near-wall particles may not be slowed down enough and slip may then occur, higher-density wall particles are used to strengthen the wall effects. The density of wall particles is increased to 6. Near the wall a thin layer is assumed where the no-slip boundary condition holds. We enforce a random velocity distribution in this layer with zero mean corresponding to a given temperature. Similar to the reflection law of Revenga et al. (1998), we further require that particles in this layer always leave the wall. The velocity of particle i in the layer is

$$\mathbf{v}_i = \mathbf{v}_\mathrm{R} + \mathbf{n}(\sqrt{(\mathbf{n}\cdot\mathbf{v}_\mathrm{R})^2} - \mathbf{n}\cdot\mathbf{v}_\mathrm{R}), \tag{12}$$

where $\mathbf{v}_\mathrm{R}$ is the random vector and $\mathbf{n}$ the unit vector normal to the wall and pointing to the flow domain. The thickness of this layer between wall and fluid particles is chosen to be the minimum between 0.5% of channel width and 0.5 of the cutoff radius. The thin layer is necessary to prevent the frozen wall to cool down the fluid and this method is more flexible when dealing with a complex geometry. In details, if i and j both denote fluid particles we choose $a_{ij} = a_\mathrm{fluid} = 18.75$ to satisfy the compressibility of water suggested by Groot and Waren (1997). When calculating the interaction between fluid and wall particles, we change the a_{ij} to obtain different wettabilities of the fluids on surface.

2.4 Stress tensor

Stress tensor components are calculated by the Irving-Kirkwood method (Fan et al. 2002; Irving and Kirkwood 1950). Here, the contribution of each particle to the stress tensor consists of two parts, a configuration part and a kinetic part:

$$S_{\alpha\beta} = -\frac{1}{V}\left\langle \sum_i^{N_p} m_i u_{i\alpha} u_{i\beta} + \sum_i^{N_p}\sum_{j>i}^{N_p} r_{ij\alpha} F_{ij\beta} \right\rangle, \tag{13}$$

where m_i is the particle mass ($m_i = 1$unit), N_p the number of particle, $u_{i\alpha}$and $u_{i\beta}$the peculiar velocity components of particle i , for example, $u_{i\alpha} = v_{i\alpha} - \overline{v}_\alpha(\mathbf{x})$, with $\overline{v}(\mathbf{x})$ being the stream velocity at position $\mathbf{x}$, and $\langle\ldots\rangle$ denotes the ensemble average. $F_{ij\beta}$ is the β-component of the force exerted on particle i by particle j. The first sum in the right hand side of Eq. (13) denotes the contribution to the stress from the momentum transfer of DPD particles. The second sum represents the contribution from the inter-particle forces. The constitutive pressure can be determined from the trace of the stress tensor:

$$p = -\frac{1}{3}\mathrm{tr}\mathbf{S} \tag{14}$$

In the present study, the stress tensor is calculated according to Eq. (13) and this stress tensor has the geometric interpretation of being a measure for the momentum change in a fixed spatial region. It is noted that this stress formulation is strictly valid only when a homogeneous stress state exists in the entire volume. Recently Shen and Atluri (2004) proposed an atomistic level stress tensor which is in a nonvoume-average form, thus does not involve *ad hoc* specification of a relevant volume. This stress tensor is validated for both homogeneous and inhomogeneous deformations, and may have more extensive applications (Shen and Atluri 2005, Ma et al. 2005 and 2006, Matsumoto et al. 2005a and 2005b).

2.5 Calculation of interfacial tension

The interfacial tension Γ_{AB} between fluid A and fluid B could be computed using the Irving-Kirkwood equation (1950),

$$\Gamma_{AB} = \int \left[p_{zz} - \frac{1}{2}(p_{xx} + p_{yy}) \right] dz, \tag{15}$$

where p_{xx}, p_{yy}, p_{zz} are the three diagonal components of the pressure tensor $(-\mathbf{S})$. The interface is parallel to the $x-y$ plane. The interfacial tension can be further expressed as,

$$\Gamma_{AB} = Q \left[\langle p_{zz} \rangle - \frac{1}{2}(\langle p_{xx} \rangle + \langle p_{yy} \rangle) \right], \tag{16}$$

where Q is the height of the simulation channel. Eq. (16) will be applied to flat interface geometry shown in Fig. 1(a). The angular brackets denote the average over the simulation run. Groot and Warren (1997) gave the best fit of the surface tension as a function of χ-parameter and N:

$$\Gamma_{AB} = (0.75 \pm 0.02)\rho k_B T r_c \chi^{0.26\pm0.01} \cdot [1 - (2.36 \pm 0.02)/\chi]^{3/2} \quad (\text{for } N = 1) \tag{17}$$

where N is the number of segments per molecule. For monomers, $N = 1$.

Jones et al. (1999) calculated the liquid/solid interfacial tension. The interface is modelled by using particles to represent the liquid and these are acted on by an external potential, which represents the effect of the solid, as shown in Fig. 1(b). The interfacial tension is given by the expression,

$$\Gamma_{AB} = Q[\langle p_{zz} \rangle - \frac{1}{2}(\langle p_{xx} \rangle + \langle p_{yy} \rangle)] + 1/A \sum_{\alpha} \sum_{i} F_{i_\alpha z} r_{i_\alpha z} + 1/A \sum_{\beta} \sum_{i} F_{i_\beta z} r_{i_\beta z}. \tag{18}$$

Here the variable α runs over all immobile particles in interface 1, and β over interface 2. In the simulations on the fluid/fluid and the fluid/solid systems forming planar interfaces, ensemble averages of the various summations appearing in eqns. (16) and (18) were computed to obtain the respective interfacial tensions.

2.6 Simulation procedure

In the present study, the initial configurations of fluid and wall particles are generated separately by a pre-processing program and read in as input data. All fluid particles are initially located at the sites of a face-centered cubic (fcc) lattice. The total number of particles depends on the size and geometry of the flow domain and the densities of the fluid and wall materials. All of the fluid phases are assumed to be of the same density, equal to 4 units. The initial velocities of fluid particles are set randomly according to the given temperature but the wall particles are frozen. At the beginning of the simulation the particles are allowed to move without applying the external force until a thermodynamic equilibrium state is reached. Then the external force field is applied to fluid particles and the nonequilibrium simulation starts. The sketch diagram of the square microchannl is shown in Fig. 2. Periodic boundary conditions are applied in the X-direction. The value of $k_B T$ is set at 1.0.

3 Results and discussion

In DPD simulations all of the parameters are scaled by DPD units. The DPD units are not defined explicitly as in MD simulation. In the present study, the scaling is much larger than that in MD. For more details, one can refer to Fan et al. (2003). The parameters adopted in the present study are shown in Table 1.

3.1 Square microchannel flows of a single fluid

In DPD method, the interfacial tension and wettability between the solid walls (W) and fluids (fluid A or fluid B) interfaces are governed entirely by the unlike parameters a_{AB}, a_{AW} and a_{BW} (Jones et al. 1999). In the present study, we first simulate flows of a single fluid in a square microchannel in order to identify the influence of repulsive parameter in imposing no-slip boundary conditions. The size of the microchannel is $-15 \le x < 15$, $-10 \le y < 10$ and $-10 \le z < 10$. A total of 63120 simple DPD particles are used, in which 48000 fluid particles are placed in the channel and 15120

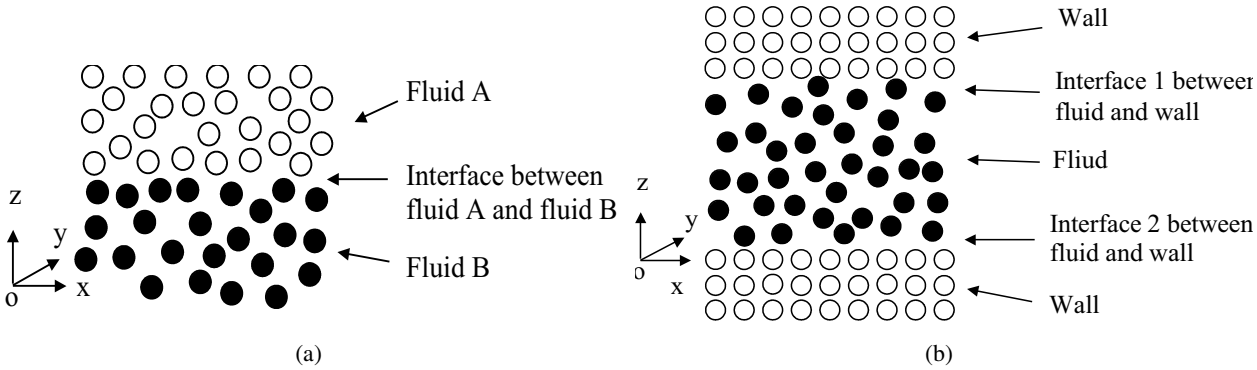

Figure 1: Calculation of interfacial tension for (a) fluid/fluid (b) fluid/solid.

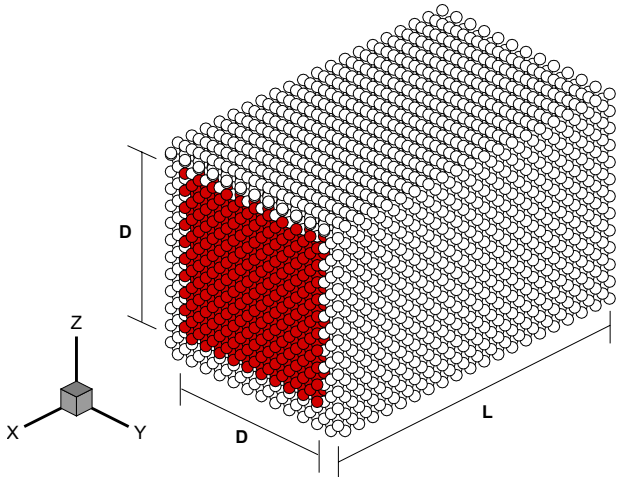

Figure 2: Sketch diagram of the square microchannel.

Table 1: Parameters adopted in the present simulation

Density	ρ	4.0
Repulsive coefficient between the same fluid	a_{AA} or a_{BB}	18.75
Dissipative coefficient	γ	4.5
Random coefficient	σ	3.0

wall particles are located in three layers of the microchannel walls. The computational domain is divided into $1\times50\times50$ bin in the x, y and z direction. All local flow properties are obtained by averaging the sampled data in each bin over10000 time steps. The time step is set at 0.01. The gravity of $g = 0.1$ is applied to each of the fluid particle.

Fig. 3 shows the fully developed velocity profile of x-velocity component in the square microchannel, in which $y = 0$ is the mid-plane of the square channel. When $g = 0.1$, the DPD simulated mass flowrate is 3416.29. Equivalently, the Reynolds number $Re(= \dot{m}/(D \cdot \mu))$ is 71.11. At $y = -6$, the computational results are compared well with the CFD solver Fluent solutions. At $y = 0$, the difference between the DPD simulation results and Fluent solution is within 2.5%.

Fig. 4 shows the influence of various fluid/wall repulsive parameters on the velocity profile in the microchannel. We can see that the no-slip boundary condition could be well held when the repulsive parameter is increased from 9.68 to 18, in which the value of $a_{\mathrm{AW}} = 9.68$ is adopted in Fan et al. (2003) and Chen et al. (2006). In fact, various wettabilities could be obtained by changing the repulsive parameter in this range for binary immiscible flow, which will be discussed later in this paper. As shown in Fan et al. (2003), when $a_{\mathrm{AW}} = 9.68$, the density profiles for a simple DPD fluid in Poiseuille flow is almost uniform across the channel except in the region near the wall, where a fluctuation in density still exists but is not as severe as that predicted by MD simulation. The temperature is almost uniform across the channel. The fluctuation may be further reduced if smaller repulsion strength of the wall particles is used.

In the present study, we can see increasing the repulsive parameter from 9.68 to 18.0 cause larger density fluctuation across the channel. The density level of the fluid in the middle of the channel is elevated and the density near the wall region is decreased, as shown in Fig 5. The temperature is almost uniform across the channel for both of these two values. Fig. 6 shows the density increasing gives rise to pressure increasing in the central part of the channel, which is what we expect.

Then we study the particle motion. We trace two kinds of fluid particles: one starts from the near-wall region and the other starts from the central part of the channel. As shown in Fig. 7, the typical motion might be described as Brownian and there is no significant difference between particles that are initially near the wall and those initially in the middle of the channel. The thermal motion eventually obliterates the initial bias. This is similar to what Koplik el al's work (1989) in MD study. In the mean time, it is also consistent with the rolling mechanism when imposing the no-slip boundary condition.

3.2 Interfacial tension

In order to compute the interfacial tension between fluid A and fluid B, the channel of $40 \times 10 \times 30$ units is divided into two layers of thickness of 15 units each, as shown in Fig. 1(a). The upper layer is filled with fluid A and the lower layer is filled with fluid B. Each layer consists of 24000 DPD particles, totalling 48000 particles in the system. Similarly, the interfacial tension between fluid and wall could be calculated with upper and lower interfaces between fluid and walls, as shown in Fig. 1(b), in which including 48000 fluid particles and 15000 wall particles.

From Groot and Warren's theoretical formula, Eq. (17), we obtain the following interfacial tension between fluid A and fluid B for monomers with $\Delta a = 37.5$ ($\Delta a = a_{\mathrm{AB}} - a_{\mathrm{AA}}$ or $a_{\mathrm{AB}} - a_{\mathrm{BB}}$ for fluid-fluid interface and $a_{\mathrm{AA}} = a_{\mathrm{BB}}$): (1) $\Gamma_{\mathrm{AB}} = 3.81$ for $\rho = 3$ and (2) $\Gamma_{AB} = 6.06$ for $\rho = 5$. The extrapolation value for our case ($\rho = 4$) is 4.94, which is close to our simulation result, Fig. 8, of 5.25 for a monomer with $\Delta a = 37.5$, $a_{\mathrm{AB}} = 56.25$, $a_{\mathrm{AA}} = a_{\mathrm{BB}} = 18.75$ and $\rho = 4$. The interfacial tension increases with increasing a_{AB} between the two fluids, as shown in Fig. 8. It also shows the interfacial tension between the solid and fluid. The fluid/solid interfacial tension is always greater than the fluid/fluid interfacial tension for the same repulsive parameters. Jones et al. (1999) calculated the interfacial tensions between two immiscible fluids and between fluid and solid surfaces with different interaction

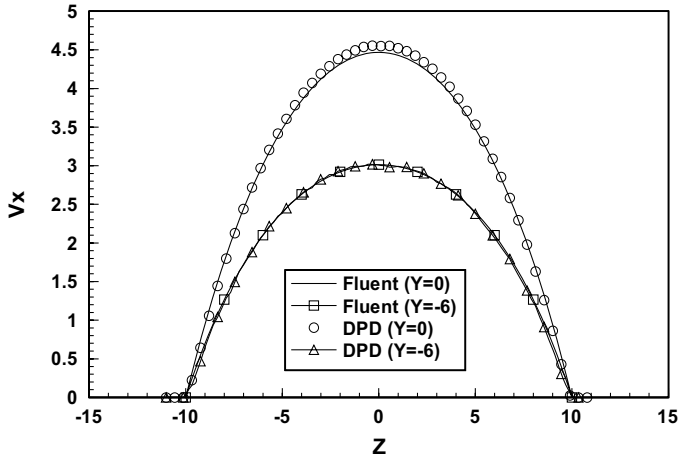

Figure 3: Comparison between current DPD calculation and Fluent simulation for fully developed velocity profile along Z direction.

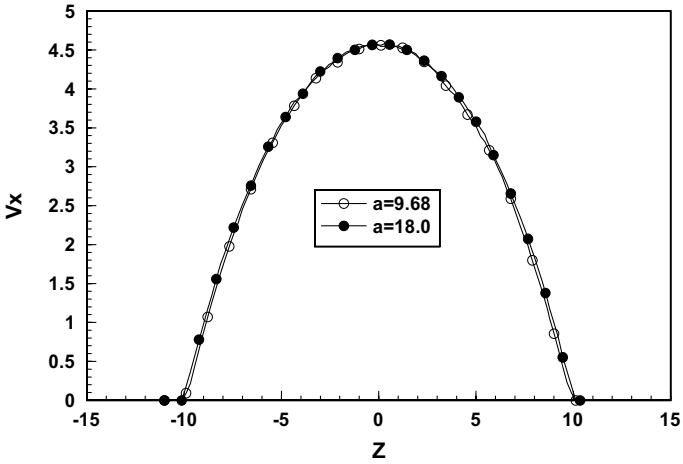

Figure 4: Fully developed velocity profile under various fluid/solid repulsive parameters.

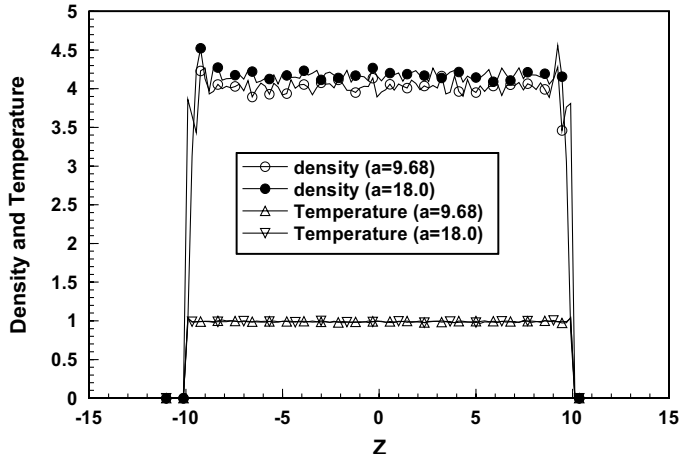

Figure 5: The density and temperature profiles of a single DPD fluid in a square microchannel (Y=0).

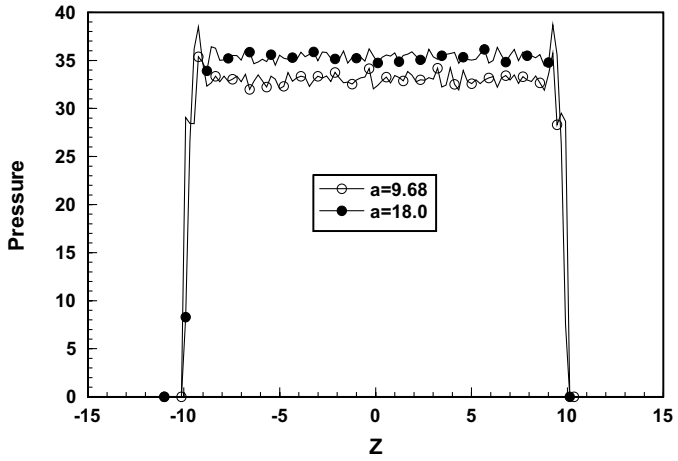

Figure 6: The pressure profiles of a simple DPD fluid in a square microchannel (Y=0).

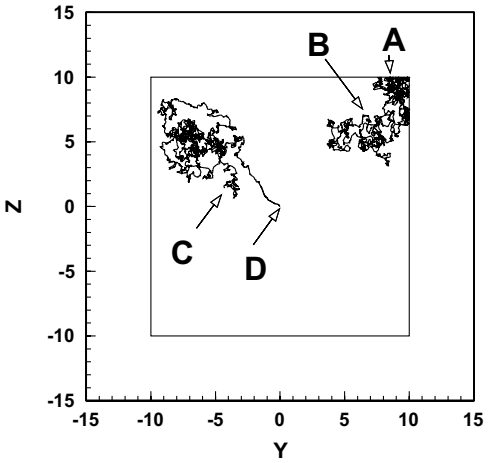

Figure 7: Particle trajectories in a square microchannel.

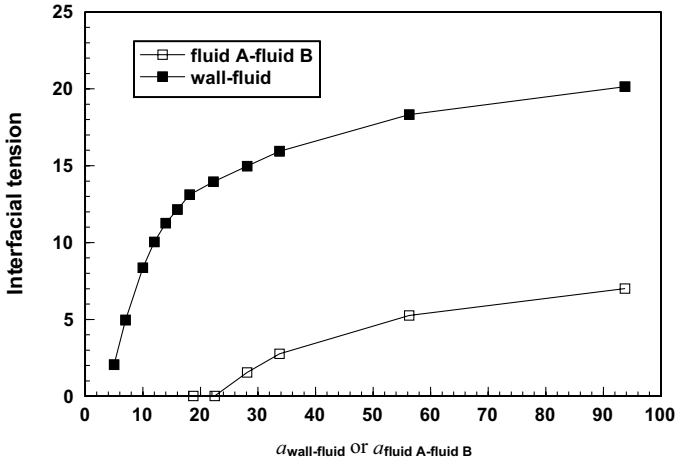

Figure 8: Calculation of interfacial tension.

parameters, same conclusions could be found in their work.

3.3 Immiscible fluids

3.3.1 Static contact angle

Groot and Warren (1997) suggested that the repulsive coefficient should be calculated as followings in order to satisfy the compressibility of water,

$$a_{ij} = 75 k_B T / \rho \tag{19}$$

They also recommend $\sigma = 3$, with $\lambda = 0.65$ in the velocity-Verlet algorithm. In the present study, we choose the fluid density $\rho = 4$ and set $k_B T = 1$. From Eq. (19), the repulsive coefficient between the same type of fluid particles is 18.75. Furthermore, the repulsive coefficient between fluid A and fluid B is increased to 56.25 to obtain binary immiscible fluids. Then we fix the repulsive coefficient $a_{\text{wall-fluid B}}$ between wall and fluid B at 10.0, while changing the repulsive parameter $a_{\text{wall-fluid A}}$ between wall and fluid A from 10.0 to 20.0. Under equilibrium conditions, the fluids retain their initial segregation, and have their corresponding contact angles, as shown in Fig. 9(a). Consider Young's equation relating the solid-liquid and liquid-liquid interfacial free energies per unit area for the configuration shown in Fig 9(b), we have

$$\Gamma_{AW} + \Gamma_{AB} \cos\theta = \Gamma_{BW}, \tag{20}$$

where the interfacial tension between fluids and between fluid and solid surface is obtained from Fig 8. Table 2 shows the comparison between the DPD simulated results and Young's equation. The maximal difference is 6.39%. It shows the DPD simulated static contact angles are in good agreement with the theoretical prediction although some differences exit due to thermal fluctuation. The higher accuracy could be achieved by increasing the size of the computational domain or increasing the sampling times in the ensemble averaging.

3.3.2 Dynamic contact angle

In the present study, the motion of a contact line is investigated by applying acceleration to each fluid particle with two kinds of g (=0.02 or 0.08, respectively). Figs. 10(b) and (c) show that the advancing and receding contact angles are different from each other when the contact line moves. In the mean time, they differ from the static angle. Similar to MD simulation (Koplic et al. 1989), the advancing angle increases and the receding angle decreases with increasing acceleration, but with large fluctuation in the simulation.

Furthermore, it is found that the fluid A is elongated more when the acceleration is larger in flow direction. As shown in Fig. 10(b) and (c), fluid A is about 16.5 long in x direction when g = 0.02, while it is about 19.5 long when g = 0.08. In order to investigate the flow behaviour, we plot the figure of fluid A seen from the cross-section of $y-z$ plane. When the contact line starts to move, the corner of the square microchannel is gradually occupied by fluid B. It shows that the cross-section area of fluid A reduces with increasing of acceleration g and its shape retracts towards the central part of the y-z plane and forms a circle. The retraction extent of the fluid A is dependant on the velocity of itself. Actually in this case, for the interaction with the solid wall, fluid A is hydrophobic and fluid B is hydrophilic. In koplic et al.'s study (1989), they noted a thin film of fluid A left behind along the parallel plate channel, in which the fluid A is hydrophilic, the film contains the fluid more strongly attracted to the wall. In the present study, we found that the effect is also very dominant when there are corners.

Fig. 12 shows moving velocity of fluid A with the repulsive coefficients, in which the acceleration is set at 0.02. The triangle in Fig. 12 represents the case of repulsive coefficient between solid wall and fluid A is varying, while the repulsive coefficient between solid wall and surrounding fluid (i.e. fluid B) is kept at 10.0. The corresponding static angle could be found in Table 2. The circle in Fig. 12 represents the case of repulsive coefficients between solid wall and both of the two kinds of fluids (fluid A and fluid B) are varying, but with the static contact kept constant at 90^o, i.e. $a_{\text{wall-fluid A}} = a_{\text{wall-fluid B}}$. It is found that for these two cases, the moving velocity increases with the increasing repulsive coefficients.

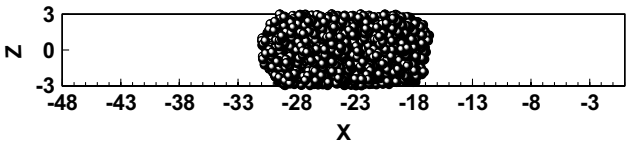

(a)

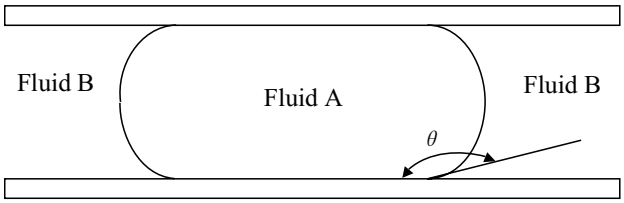

(b)

Figure 9: Static contact angle.

Table 2: Comparison between the DPD simulation and Young's equation

$a_{\text{wall-fluid A}}$	$a_{\text{wall-fluid B}}$	Contact angle (DPD)	Contact angle (Young)
10	10	89°	90°
12	10	116°	109.03°
14	10	125°	123.73°
16	10	135°	136.2°
18	10	149°	153.28°
20	10	164°	167.98°

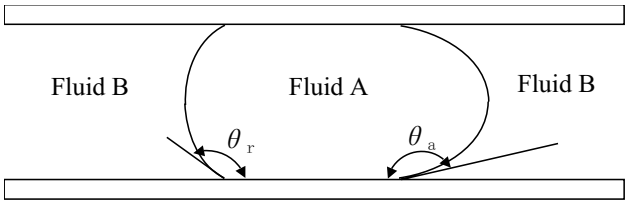

(a)

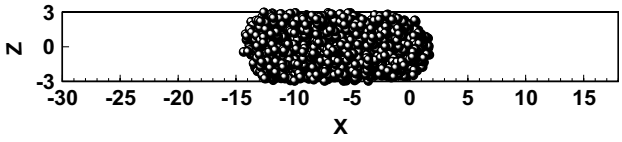

(b) $g = 0.02$

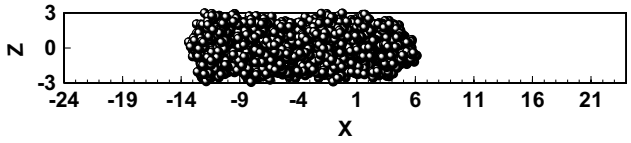

(c) $g = 0.08$

Figure 10: The advancing and receding angle with moving contact line.

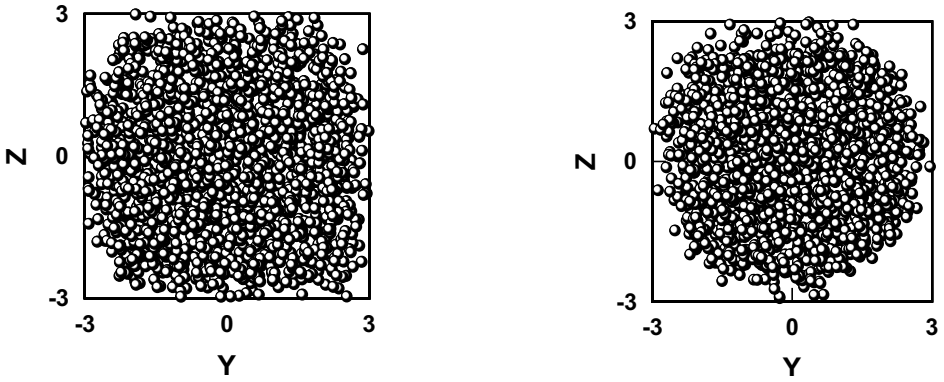

(a) (b)

Figure 11: Flow shape of fluid A in $y-z$ plane. (a) $g = 0.02$, (b) $g = 0.08$.

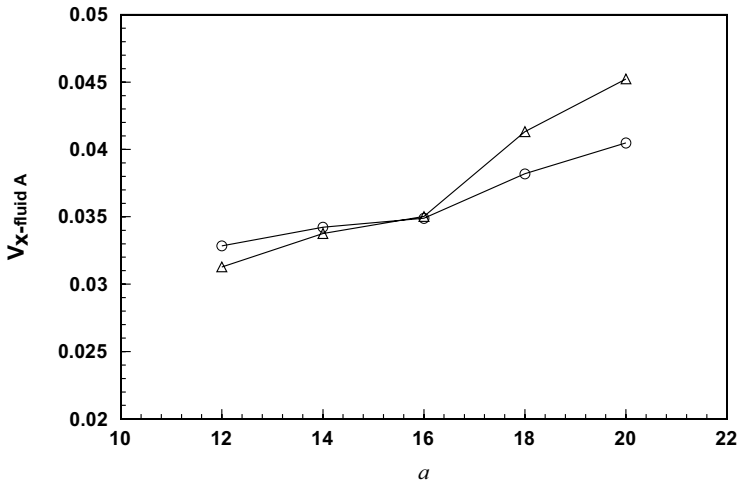

a

Figure 12: Moving velocity of fluid A with the repulsive coefficient.

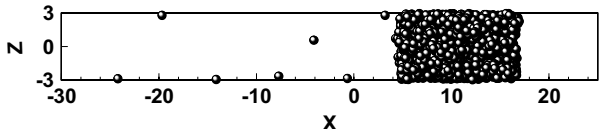

Figure 13: Escaping of some particles from fluid A.

In closer scrutiny, we have found that the no-slip boundary condition could be well held for single fluid in the square microchannel when the repulsive coefficient varies between 9.68 and 18.0. Under this condition, it is observed for immiscible binary fluids that the flow velocity of the fluid A in the microchannel could be increased by increasing the repulsive coefficient while its static contact angle is unchanged. Due to the thermal fluctuation, we can see some particles escape from fluid A and enter into fluid B, as shown in Fig. 13.

It is also noted in Fig. 12 that at the lower value of repulsive coefficient, the moving velocity of fluid A for the above two mentioned cases has no significant difference from each other, the little difference could be attributed to the limit statistical resolution. When the repulsive coefficient is increased to 20, where the triangle representing the static contact angle is at 164^{o} (i.e. hydrophobic) and the circle still representing the static contact angle at90^{o}, it could be seen that the hydrophobic fluid entails faster motion. Larger static angle

may produce larger moving velocity.

4 Conclusions

In the present study, we investigated the fluids flow in a square microchannel using the dissipative particle dynamics method. It is found that the DPD simulated velocity distribution of single fluid in square microchannel is in good agreement with the Fluent solutions. The no-slip boundary condition could be well held when the repulsive coefficient is varied from 9.68 to 18, while various wettabilities could be obtained by changing the repulsive parameters in this range for binary immiscible flow. The typical motion of the particle might be described as Brownian. The interfacial tension is calculated and it shows that the simulated interfacial tension is in accord with Groot et al's theoretical prediction. With the same repulsive coefficient, the interfacial tension between the solid and fluid is always greater than the fluid/fluid interfacial tension, which is similar to Jones et al.'s conclusions (1999). The calculated static contact angle with present DPD method is in agreement with Young's equation. It is found under the condition of moving contact line, not only the advancing and receding contact angle are different from each other, but also the cross-section area of hydrophobic fluid is retracted toward the central part of the square microchannel and forms a circle. The retraction extent of the hydrophobic is dependant on the velocity itself. For immiscible fluid, the moving velocities of hydrophobic fluid A in the microchannel could be increased by increasing the repulsive coefficient, and larger static angle may produce larger moving velocity.

Acknowledgement: Support given by the Research Grants Council of the Government of the HKSAR under Grant Nos. PolyU 5221/05E and 5231/06E and by the National Natural Science Foundation of China under Grant No. 50576051 is gratefully acknowledged.

References

Abrahamse, A.J., van der Padt, A. and Boom, R.M. (2001): Process fundamentals of membrane emulsification: simulation with CFD, *AIChE Journal*, vol. 47, pp. 1285-1291.

Barrat, J.L. and Bocquet, L. (1999): Large slip effect at a nonwetting fluid-solid interface, *Physical Review Letters,* vol. 82, pp. 4671-4674.

Bringer, M.R., Gerdts, C.J., Song, H., Tice, J.D. and Ismagilov, R.F. (2004): Microfluidic systems for chemical kinetics that rely on chaotic mixing in droplets, *Philosophical Transactions of The Royal Society of London Series A-Mathematical Physical and Engineering Sciences*, vol. 362, pp. 1087-1104.

Chen, S., Phan-Thien, N., Khoo, B.C. and Fan, X.J. (2006): Flow around spheres by dissipative particle dynamics, *Phys. Fluids*, vol. 18, 103605.

Chen, S., Phan-Thien, N., Fan, X.J. and Khoo, B.C. (2004): Dissipative particle dynamics simulation of polymer drops in a periodic shear flow, *Journal of Non-Newtonian Fluid Mechanics,* vol. 118, pp. 65-81.

Clark, A.T., Lal, M., Ruddock, J.N. and Warren, P.B. (2000): Mesoscopic simulation of drops in gravitational and shear fields, *Langmuir,* vol. 16, pp. 6342-6350.

Croce, G. and D'Agaro, P. (2005): Numerical simulation of roughness effect on microchannel heat transfer and pressure drop in laminar flow, *Journal of Physics D-Applied Physics,* vol. 38, pp. 1518-1530.

Duong-Hong, D., Phan-Thien, N. and Fan, X.J. (2004): A implementation of no-slip boundary conditions in DPD, *Computational Mechanics,* vol. 35, pp. 24-29.

Elliott, J.A. and Windle, A.H. (2000): A dissipative particle dynamics method for modelling the geometrical packing of filler particles in polymer composites, *Journal of Chemical Physics,* vol. 113, pp. 10367-10376.

Español, P. and Warren, P. (1995): Statistical mechanics of dissipative particle dynamics, *Europhysics Letters*, vol. 30, pp. 191-196.

Fan, X.J., Phan-Thien, N., Chen, S., Ng, T.Y. and Wu, X.H. (2006): Simulating DNA molecular suspension flow using dissipative particle dynamics, *Physics of Fluids*, vol. 18, 063102.

Fan, X.J., Phan-Thien, N., Ng, T.Y., and Xu, D. (2002): Molecular dynamics simulation of a liquid in a complex nanochannel flow, *Phys. Fluids*, vol. 14, pp. 1146-1153.

Fan, X.J., Phan-Thien, N., Yong, N.T., Wu, X.H. and Xu, D. (2003): Microchannel flow of a macromolecular suspension, *Physics of Fluids*, vol. 15, pp. 11-21.

Frisch, U., Hasslacher, B. and Pomeau, Y. (1986): Lattice-gas automata for the Navier-Stokes equations, *Physical Review Letters*, vol. 56, pp. 1505-1508.

Gau, H., Herminghaus, S., Lenz, P. and Lipowsky, R. (1999): Science, vol. 283, pp. 46-49.

Groot, G.D. and Warren, P.B. (1997): Dissipative particle dynamics: Bridging the gap between atomistic and mesoscopic simulation, *Journal of Chemical Physics*, vol. 107, pp. 4423-4435.

Hoogerbrugge, P.J. and Koelman, J.M.V.A. (1992): Simulating microscopic hydrodynamic phenomena with dissipative particle dynamics, *Europhysics Letters,* vol. 19, pp. 155-160.

Huilgol, R.R. and Phan-Thien, N. (1997): Fluid mechanics of viscoelasticity: general principles, constitutive modelling, analytical and numerical techniques, Elsevier, Amsterdam.

Hur, J.S., Shaqfeh, E.S.G. and Larson, R.G. (2000): Brownian dynamics simulations of single DNA molecules in shear flow, *Journal of Rheology,* vol. 44, pp. 713-742.

Irving, J.H. and Kirkwood, J.G. (1950): The statistical mechanical theory of transport processes. IV. The equations of hydrodynamics, *Journal of Chemical Physics*, vol. 18 pp. 817-829.

Jones, J.L., Lal, M., Ruddock, J.N. and Spenley, N.A. (1999): Dynamics of a drop at a liquid/solid interface in simple shear fields: A mesoscopic simulation study, *Faraday Discussions,* vol. 112, pp. 129-142.

Koplik, J. Banavar, J.R. and Willemsen, J.F. (1989): Molecualr dynamics of fluid flow at solid surfaces, *Phys of Fluids,* vol. A 1, pp. 781-794.

Kuksenok, O., Yeomans, J.M. and Balazs, A.C. (2002): Using patterned substrates to promote mixing in microchannels, *Physical Review E,* vol. 65, Art. No. 031502 Part 1.

Kuksenok, O., Jasnow, D., Yeomans, J. and Balazs, A.C. (2003): Periodic droplet formation in chemically patterned microchannels, *Physical Review Letters*, vol. 91, Art. No. 108303.

Lauga, E., Brenner, M.P. and Stone, H.A. (2005): Microfluidics: the no-slip boundary condition, in Foss, Tropea and Yarin (eds.): *Handbook of Experimental Fluid Dynamics*, Springer, New-York.

Lee, J. and Kim, C.J. (2000): Surface-tension-driven microactuation based on continuous electrowetting, *Journal of Microelectromechanical Systems,* vol. 9, pp. 171-180.

Liu, Y., Yang, X.Z., Yang, M.J. and Ting, L. (2004): Mesoscale simulation on the shape evolution of polymer drop and initial geometry influence, *Polymer,* vol. 45, pp. 6985-6991.

Ma, J., Liu, Y., Liu, H.B. and Komanduri R. (2006): Multiscale simulation of nanoindentation using the generalized interpolation material point (GIMP) method, dislocation dynamics (DD) and molecular dynamics (MD), *CMES-Computer Modeling in Engineering & Sciences*, vol. 16, pp. 41-55.

Ma, J., Lu, H., Wang, B., Roy, S., Hornung., R., Wissink, A. and Komanduri, R. (2005): Multiscale simulations using generalized interpolation material point (GIMP) method and SAMRAI parallel processing, *CMES-Computer Modeling in Engineering & Sciences*, vol. 8, pp. 135-152.

Marsh, C. (1998): Theoretical aspect of dissipative particle dynamics, Ph. D. Dissertation, University of Oxford.

Matsumoto, R. and Nakagaki, M. (2005a): Estimation of the mechanical properties of amorphous metal with a dispersed nano-crystalline particle by molecular dynamics simulation, *CMES-Computer Modeling in Engineering & Sciences*, vol. 10, pp. 187-197.

Matsumoto, R., Nakagaki, M., Nakatani, A. and Kitagawa, H. (2005b): Molecular-dynamics study on crack growth behavior relevant to crystal nucleation in amorphous metal, *CMES-Computer*

Modeling in Engineering & Sciences, vol. 9, pp. 75-84.

Novik, K.E. and Coveney, P.V. (1997): Using dissipative particle dynamics to model binary immiscible fluids, *International Journal of Modern Physics C,* vol. 8, pp. 909-918.

Pivkin, I.V. and Karniadakis, G.E. (2005): A new method to impose no-slip boundary conditions in dissipative particle dynamics, *Journal of Computational Physics,* vol. 207, pp. 114-128.

Revenga, M., Zuniga, I. and Español, P. (1999): Boundary conditions in dissipative particle dynamics, *Computer Physics Communications*, vol. 121-122, pp. 309-311.

Revenga, M., Zuniga, I. and Español, P. (1998): Boundary models in DPD, *International Journal of Modern Physics C*, vol. 9 pp. 1319-1328.

Shen, S.P. and Atluri, S.N. (2005): A tangent stiffness MLPG method for atom/continuum multiscale simulation, *CMES: Computer Modeling in Engineering & Sciences*, vol. 7, pp. 49-67.

Shen, S.P. and Atluri, S.N. (2004): Atomic-level stress calculation and continuum-molecular system equivalence, *CMES: Computer Modeling in Engineering & Sciences*, vol. 6, pp. 91-104.

Sugiura, S., Nakajima, M. and Seki, M. (2002a): Effect of channel structure on microchannel emulsification, *Langmuir*, vol. 18, pp. 5708-5712.

Sugiura, S., Nakajima, M. and Seki, M. (2002b): Prediction of droplet diameter for microchannel emulsification, *Langmuir,* vol. 18, pp. 3854-3859.

Suppa, D., Kuksenok, O. and Balazs, A.C. (2002): Phase separation of a binary fluid in the presence of immobile particles: A lattice Boltzmann approach, *Journal of Chemical Physics*, vol. 116, pp. 6305-6310.

Tang, G.H., Tao, W.Q. and He, Y.L. (2005): Three-dimensional lattice Boltzmann model for gaseous flow in rectangular microducts and microscale porous media, *Journal of Applied Physics,* vol. 97, Art. No. 104918 Part 1.

Visser, D.C., Hoefsloot, H.C.J. and Iedema, P.D. (2005): Comprehensive boundary method for solid walls in dissipative particle dynamics, *Journal of Computational Physics,* vol. 205, pp. 626-639.

Vladisavljevic, G.T. and Williams, R.A. (2005): Recent developments in manufacturing emulsions and particulate products using membranes, *Advances in Colloid and Interface,* vol. 113, pp. 1-20.

Willemsen, S.M., Hoefsloot, H.C.J. and Iedema, P.D. (2000): No-slip boundary condition in dissipative particle dynamics, *International Journal of Modern Physics C,* vol. 11, pp. 881-890.

Zhang, K., Manke, C.W., Madden, W.G., and Schlijper, A.G. (1997): Modelling the rheology of polymer solutions by dissipative particle dynamics, *Tribol. Lett*. Vol. 3, pp. 133-138.